Quantification of the electron donating capacity and UV absorbance of dissolved organic matter during ozonation of secondary wastewater effluent by an assay and an automated analyzer

Author(s):
Walpen, Nicolas; Houska, Joanna; Salhi, Elisabeth; Sander, Michael; von Gunten, Urs

Publication date:
2020-10-15

Permanent link:
https://doi.org/10.3929/ethz-b-000432833

Originally published in:
Water Research 185, https://doi.org/10.1016/j.watres.2020.116235

Water Research 185 (2020) 116235

Contents lists available at ScienceDirect

Water Research

journal homepage: www.elsevier.com/locate/watres

Quantification of the electron donating capacity and UV absorbance of dissolved organic matter during ozonation of secondary wastewater effluent by an assay and an automated analyzer

Nicolas Walpen[a], Joanna Houska[a,c], Elisabeth Salhi[a], Michael Sander[b], Urs von Gunten[a,b,c,*]

[a] Swiss Federal Institute of Aquatic Science and Technology (Eawag), 8600 Dübendorf, Switzerland
[b] Institute of Biogeochemistry and Pollutant Dynamics, ETH Zurich, 8092 Zurich, Switzerland
[c] School of Architecture, Civil and Environmental Engineering (ENAC), Ecole Polytechnique Fédérale de Lausanne (EPFL), 1015 Lausanne, Switzerland

ARTICLE INFO

Article history:
Received 2 April 2020
Revised 30 June 2020
Accepted 25 July 2020
Available online 26 July 2020

Keywords:
Secondary-treated wastewater
Ozonation
Micropollutant abatement
Electron donating capacity
UV absorbance

ABSTRACT

Ozonation of secondary wastewater treatment plant effluent for the abatement of organic micropollutants requires an accurate process control, which can be based on monitoring ozone-induced changes in dissolved organic matter (DOM). This study presents a novel automated analytical system for monitoring changes in the electron donating capacity (EDC) and UV absorbance of DOM during ozonation. In a first step, a quantitative photometric EDC assay was developed based on electron-transfer reactions from phenolic moieties in DOM to an added chemical oxidant, the radical cation of 2,2′-azino-bis(3-ethylbenzothiazoline-6-sulfonate) ($ABTS^{\cdot+}$). The assay is highly sensitive (limit of quantification ~0.5 $mg_{DOC} \cdot L^{-1}$) and EDC values of model DOM isolates determined by this assay were in good agreement with values determined previously by mediated electrochemical oxidation (slope = 1.01 ± 0.07, R^2 = 0.98). In a second step, the photometric EDC measurement method was transferred onto an automated fluidic system coupled to a photometer (EDC analyzer). The EDC analyzer was then used to monitor changes in EDC and UV absorbance of secondary wastewater effluent treated with ozone. While both parameters exhibited a dose-dependent decrease, a more pronounced decrease in EDC as compared to UV absorbance was observed at specific ozone doses up to 0.4 $mg_{O3} \cdot g_{DOC}^{-1}$. The concentration of 17α-ethinylestradiol, a phenolic micropollutant with a high ozone reactivity, decreased proportionally to the EDC decrease. In contrast, abatement of less ozone-reactive micropollutants and bromate formation started only after a pronounced initial decrease in EDC. The on-line EDC analyzer presented herein will enable a comprehensive assessment of the combination of EDC and UV absorbance as control parameters for full-scale ozonation.

1. Introduction

Ozonation of secondary wastewater treatment plant (WWTP) effluents combined with biological post-treatment is a widely recognized strategy for abating a broad range of organic micropollutants of environmental concern (Eggen et al., 2014; Oulton et al., 2010; Patel et al., 2019; Prasse et al., 2015; von Gunten, 2018). A number of comprehensive tests in pilot- (Gerrity et al., 2011; Huber et al., 2005; Knopp et al., 2016; Snyder et al., 2006; Ternes et al., 2003) and full-scale treatment systems (Bourgin et al., 2018; Hollender et al., 2009; Zimmermann et al., 2011) have demonstrated the efficacy and feasibility of ozonation for decreasing the load of organic micropollutants discharged into surface waters. Numerous wastewater treatment plants (WWTPs) in Europe are therefore upgrading their treatment trains to include full-scale ozonation systems (VSA, 2020). However, a key challenge for the operation of these systems remains the real-time control of the ozone dosage to simultaneously meet the treatment objectives and water quality requirements.

Treatment objectives of ozonation are the abatement of selected indicator substances. For example, regulatory frameworks of au-

Abbreviations: a_λ, absorption coefficent (cm^{-1}) at the wavelength λ; ABTS, 2,2′-azino-bis(3-ethylbenzothiazoline-6-sulphonate); $ABTS^{\cdot+}$, radical cation of ABTS; DOC, dissolved organic carbon; DOM, dissolved organic matter; EDC, electron donating capacity; E_H, reduction potential reported against the standard hydrogen electrode; $\varepsilon(\lambda)$, molar absorption coefficient at the wavelength λ; LOQ, limit of quantification; MEO, mediated electrochemical oxidation; $SUVA_\lambda$, specific UV absorbance at the wavelength λ; WWTP, wastewater treatment plant.

* Corresponding author.
E-mail address: vongunten@eawag.ch (U. von Gunten).

https://doi.org/10.1016/j.watres.2020.116235

thorities in Switzerland (Federal Office for the Environment, 2018) and California (California Environmental Protection Agency, 2018) define abatement targets for specific indicator substances. The treatment objectives specified by the Swiss Federal Office for the Environment demand an average abatement of 80% for a suite of indicator substances from raw wastewater to WWTP effluent, which requires the application of minimum specific ozone doses (Bourgin et al., 2018). At the same time, water quality requirements limit the upper value for ozone exposures (i.e., $\int c_{O3}\ dt$) due to the formation of undesired oxidation by-products which are not degraded during biological post-treatment (Hollender et al., 2009; Zimmermann et al., 2011). In particular, high ozone exposures in bromide-containing waters lead to the undesired formation of bromate, a regulated, potentially carcinogenic compound (Soltermann et al., 2016; Soltermann et al., 2017; von Gunten and Hoigné, 1994). Furthermore, energy demand for ozone production also incentivizes lower ozone doses (Katsoyiannis et al., 2011). To balance these treatment objectives and water quality requirements, an accurate, real-time determination of the optimal ozone dose based on robust control parameters is critical.

In drinking water treatment, oxidant exposures have been applied successfully as control parameters (Kaiser et al., 2013). During ozonation, organic micropollutants may either be transformed by ozone or hydroxyl radicals which are transiently formed by reactions of ozone with the water matrix (Buffle et al., 2006a). The rate at which individual organic micropollutants are transformed is therefore a function of (i) the second-order rate constants of the reactions of the micropollutants with ozone and hydroxyl radical and (ii) the ozone and hydroxyl radical exposures (i.e., $\int c_{O3} dt$ and $\int c_{\cdot OH} dt$) (Buffle et al., 2006b). While ozone and hydroxyl radical exposures can be determined on-line during drinking-water ozonation (Kaiser et al., 2013), technical limitations of current analytical instrumentation prohibits quantifying the same parameters during ozonation of secondary WWTP effluents due to fast ozone depletion (Buffle et al., 2006b).

To circumvent this obstacle in wastewater treatment, surrogate parameters associated with readily observable changes in the properties of dissolved organic matter (DOM) have been suggested as control parameters for ozonation. In this context, ozone-induced transformations of chromophoric moieties in DOM (Buffle et al., 2006a; Wenk et al., 2013), have received a lot of attention. Ozone-induced decreases in absorbance at 254 nm were found to correlate with the abatement of different classes of organic micropollutants (Bahr et al., 2007; Nanaboina and Korshin, 2010; Wert et al., 2009; Wittmer et al., 2015) and viruses (Wolf et al., 2019). Therefore, the relative decrease in UV absorbance allows to assess micropollutant abatement on-line and is considered a suitable control parameter for full-scale ozonation (Gerrity et al., 2012; Park et al., 2017; Pisarenko et al., 2012; Stapf et al., 2016; Wittmer et al., 2015). Recently, empirical models were proposed that additionally incorporate changes in total DOM fluorescence to improve previous process control systems (Chys et al., 2017; Gamage et al., 2013; Park et al., 2017). However, absorbance values measured at 254 nm primarily predict the content of aromatic carbon in DOM (Weishaar et al., 2003) and thus only provide limited information on the ozone reactivity of DOM. Therefore, the application of an additional, complementary control parameter based on decreases in the content of ozone-reactive DOM moieties would provide a more robust process control system based on two independent parameters.

A promising complementary approach is the quantification of the electron donating capacity (EDC) of DOM, which provides a measure for the phenol content of DOM (Aeschbacher et al., 2010). The EDC is operationally defined as the number of electrons transferred from electron-donating moieties in DOM to a chemical oxidant at a defined reduction potential (E_H) and pH within a certain reaction time. Previous studies used the radical cation of 2,2′-azino-bis(3-ethylbenzothiazoline-6-sulphonate) ($ABTS^{\cdot+}$) as chemical oxidant (Aeschbacher et al., 2012; Chon et al., 2015; Walpen et al., 2016) because (i) $ABTS^{\cdot+}$ is reversibly reduced in a pH-independent one-electron transfer and (ii) the standard reduction potential of the redox couple $ABTS^{\cdot+}$/ABTS ($E_H{}^0 = +0.68$ V (Scott et al., 1993)) is sufficiently high to allow for the oxidation of phenolic moieties in DOM. Ozonation of DOM samples, including model DOM isolates, surface water and WWTP effluents, resulted in decreasing EDC values with increasing specific ozone doses (Önnby et al., 2018b; Wenk et al., 2013), consistent with the ozone-induced transformation of phenolic DOM moieties forming e.g., quinones and ring cleavage products via the Criegee mechanism (Ramseier and von Gunten, 2009; Tentscher et al., 2018). Recently, the potential application of changes in EDC as control parameter for ozonation was demonstrated in laboratory experiments (Chon et al., 2015). Wastewater effluent samples, which were exposed to increasing ozone doses exhibited pronounced, dose-dependent decreases in EDC, which correlated with the abatement of selected organic micropollutants with different ozone reactivities. Taken together, these findings warrant further investigations on the applicability of EDC as control parameter for ozonation. However, these existing methods are not suited for such an application.

EDC values have previously been determined by mediated electrochemical oxidation (MEO) (Aeschbacher et al., 2010). Subsequent development of analytical methods based on size-exclusion chromatography coupled to a post-column reaction with $ABTS^{\cdot+}$ (Chon et al., 2015; Önnby et al., 2018b) and flow-injection analysis (Önnby et al., 2018b; Walpen et al., 2016) significantly enhanced the sensitivity for EDC quantification, a requirement for analyzing solutions with low DOM contents. While these analytical methods already introduced some degree of automation (i.e., automatic sample injection), they were not designed for a continual, long-term process monitoring. The primary reasons prohibiting the application of these methods for long-term monitoring are (i) the long delay times from sampling to obtaining EDC values, (ii) the requirement of advanced chromatographic or electrochemical instrumentation resulting in high investment costs and frequent maintenance, and (iii) high reagent consumption rates. Recently, a simple, field-deployable, photometric EDC method was presented (Yuan et al., 2019). Even though the method was not automated, the study demonstrated the potential for on-site photometric EDC measurements of DOM in natural and engineered systems.

The objective of this study was to develop an automated EDC analyzer for monitoring relative changes in EDC and the UV absorbance of DOM during ozonation of secondary WWTP effluents. To this end, a photometric EDC assay was developed by adapting existing EDC methods and comprehensively validated. In a subsequent step, this method was implemented on an automated fluidic system, the EDC analyzer. In a third step, the performance of the EDC analyzer was assessed by measuring changes in EDC of a secondary WWTP effluent during ozonation and the resulting decreases in EDC were compared to changes in UV absorbance and the abatement of selected organic micropollutants. In a fourth and final step, the applicability of the combination of EDC and UV absorbance as control parameters for ozonation was evaluated.

2. Materials and methods

2.1. Chemicals

A list of the chemicals used in this study (including information on their purity and supplier) is provided in Section S1.1 of the Supplementary Information (SI). All aqueous solutions were prepared

in ultra-pure water with a resistivity of >18.2 MΩ·cm (Barnstead NanoPure, Thermo Scientific, Switzerland).

2.2. Dissolved organic matter samples

2.2.1. Model DOM isolates

Six model DOM isolates were purchased from the International Humic Substances Society (St. Paul, Minnesota, USA): Nordic Lake Reference Fulvic Acid (NLFA, 1R105F), Pony Lake Reference Fulvic Acid (PLFA, 1R109F), Pahokee Peat Standard Humic Acid (PPHAS, 1S103H), Suwannee River II Standard Fulvic Acid (SRFA, 2S101F), Suwannee River II Standard Humic Acid (SRHA, 2S101H), and Suwanee River I Aquatic Natural Organic Matter (SRNOM, 1R101N). These model DOM isolates were selected because their EDC values (i) were determined previously by MEO (Aeschbacher et al., 2012) and (ii) cover a wide range due to the different origins of the DOM samples. Stock solutions ($c_{DOC} \cong 50\ mg_{DOC} \cdot L^{-1}$) of these model DOM isolates were prepared by dissolving the isolates in water while adding sodium hydroxide solution (0.1 M) to maintain a pH of 6.5 ± 0.5.

2.2.2. Secondary WWTP effluent samples

Grab samples were collected at the municipal WWTP Werdhölzli in Zurich, Switzerland, where conventional secondary clarification is followed by ozonation and sand filtration for biological post-treatment (details on the treatment processes are provided in Section S1.2 and **Fig. S1**, SI). The wastewater samples were collected from three different points in the treatment process: (i) the ozonation-reactor influent, (ii) the ozonation-reactor effluent, and (iii) the sand-filter effluent. To approximately collect the same wastewater parcel in all three locations, the sampling times for sample (ii) and (iii) accounted for the hydraulic retention time of 28 and 15 min in the ozonation reactor and sand filter, respectively (calculated based on reactor volumes and flow rates). Relevant ozonation process parameters for the week before, during, and after sampling are provided in **Figs. S2** and **S3** (SI). The grab samples were filtered within two hours of collection using pre-rinsed cellulose-nitrate membranes (0.45-µm pore size, Sartorius Stedim Biotech, Germany) to remove suspended particles potentially causing abrasion in the valve and syringe pump of the EDC analyzer (see Section 2.6.3). Concentrations of DOC, nitrite and ammonium as well as pH and alkalinity of these wastewater samples are provided in **Table S1** (SI).

2.3. Characterization of DOM samples

UV–visible light absorbance spectra ($200 \leq \lambda \leq 800$ nm) of DOM solutions were measured on a spectrophotometer (Cary 100, Varian, USA) in 10-mm quartz cuvettes (Hellma, Germany). Dissolved organic carbon (DOC) concentrations (LOQ = 0.5 $mg_{DOC} \cdot L^{-1}$, measurement error: 0.2 $mg_{DOC} \cdot L^{-1}$) were quantified on a total organic carbon analyzer (TOC-L CSH, Shimadzu, Japan). The quantification methods for alkalinity as well as nitrite and ammonium concentrations are described in Section S1.4 (SI).

2.4. Preparation of ozone stock solutions

Ozone was produced using a laboratory ozone generator (803 BT, BMT, Germany) fed with oxygen gas (>99.995%). Ozone stock solutions ($c_{O3} \cong 1.5$ mM) were prepared by continuously sparging the ozone-containing gas through water cooled on ice (Bader and Hoigné, 1981). The dissolved ozone concentration in the ozone stock solution was determined photometrically from 5-fold diluted, acidified aliquots (40 mM phosphoric acid) using a molar absorption coefficient of $\varepsilon(260\ nm) = 3'200\ M^{-1}cm^{-1}$ (von Sonntag and von Gunten, 2012, chap. 2.5).

2.5. Ozonation of secondary WWTP effluent containing micropollutants

Increasing doses of ozone were added to the ozonation-reactor influent sample to (i) demonstrate the analytical performance of the EDC analyzer with a real, secondary WWTP effluent and (ii) to assess the predictive power of relative changes in EDC and UV for micropollutant abetment. For this purpose, three micropollutants (17α-ethinylestradiol, bezafibrate, and atrazine) were each added to a separate aliquot of the filtered, secondary WWTP effluent. The starting concentration of each micropollutant was 1 ± 0.05 µM. While this concentration is higher than the concentrations typically observed for these compounds in secondary WWTP effluents, the relative abatement of these compounds was shown to be independent of the initial micropollutant concentration as long as the added micropollutants do not significantly affect the ozone and hydroxyl radical exposures (Zimmermann et al., 2011). At this starting concentration, each micropollutant only contributed slightly to the scavenging of ozone (<3%) or hydroxyl radicals (< 6%) by the sample matrix (see Section S1.5, SI, for the estimation of the scavenging contribution). These micropollutants were selected to span a wide range of reactivities towards ozone (**Table S2**, SI). A fourth aliquot was prepared to which no micropollutants were added. Subsequently, ozone stock solution was added to the four aliquots of the secondary WWTP effluent at increasing specific ozone doses (0–0.9 $mg_{O3} \cdot mg_{DOC}^{-1}$) at a temperature of 23 ± 1 °C under stirring. These ozonated samples were then stored at room temperature for >24 h to guarantee full ozone depletion before analysis. EDC, UV absorbance, as well as bromide and bromate concentrations were quantified in the micropollutant-free aliquot to avoid potential interferences from the presence of added micropollutants. Accounting for the volume of the added micropollutant- and ozone-containing solutions, the DOC concentration of this secondary WWTP effluent was diluted to 5.5 $mg_{DOC} \cdot L^{-1}$ for these laboratory ozonation experiments and was assumed to remain constant during ozonation (von Sonntag and von Gunten, 2012).

2.6. Quantification of EDC values of DOM samples

To quantify the EDC of DOM sample solutions, we developed and validated a photometric EDC assay and subsequently implemented this assay on an automated fluidic system, the EDC analyzer. The reagent and buffer solutions as well as the detailed experimental procedure for the EDC assay and EDC analyzer are described in the following paragraphs.

2.6.1. Reagent and pH buffer solutions for the EDC assay and analyzer

For both, the EDC assay and EDC analyzer, an ABTS- and a chlorine-containing solution and a pH buffer solution were prepared weekly and stored at room temperature protected from light. The ABTS-containing solution was made by dissolving ABTS (1 mM final concentration) in dilute sulfuric acid (7.5 mM, pH = 2.0). The chlorine-containing solution (1 mM final concentration) was prepared by diluting a concentrated hypochlorite stock solution in water. Chlorine concentrations were determined photometrically from alkaline aliquots (pH 11) using the molar absorption coefficient of hypochlorite $\varepsilon(292\ nm) = 359\ M^{-1}cm^{-1}$ (Wang et al., 2012). The stability of the chlorine and ABTS stock solutions was confirmed photometrically (data not shown). The pH buffer solution contained 500 mM of phosphate and resulted in a pH of 7.0 in the final reaction mixture of the EDC assay and analyzer.

2.6.2. Experimental procedure of the EDC assay

The EDC assay was adapted from existing photometric methods for quantifying EDC values of DOM (Walpen et al., 2016;

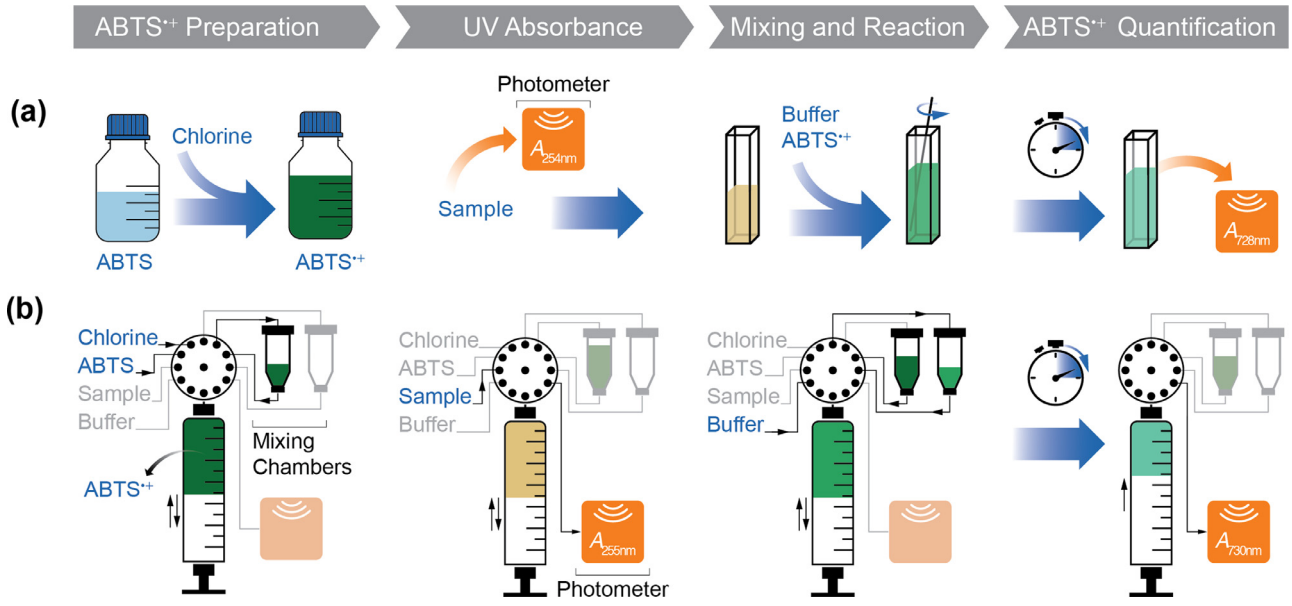

Fig. 1. Schematic representation of the two analytical methods used to quantify the electron donating capacity (EDC) and UV absorbance of dissolved organic matter (DOM) samples. **(a)** The EDC assay consisted of four steps: First, an $ABTS^{\cdot+}$-containing reagent solution was prepared by adding a chlorine solution to an ABTS-containing solution, resulting in the oxidation of ABTS to $ABTS^{\cdot+}$. Second, the absorbance of the undiluted DOM sample was measured at 254 nm. Third, a phosphate buffer solution and an aliquot of the $ABTS^{\cdot+}$-reagent solution were mixed with the DOM sample solution in a disposable cuvette. Fourth, the absorbance at 728 nm was measured after a reaction time of 15 min. **(b)** On the EDC analyzer, the same analytical procedure is executed automatically by a valve and syringe-pump system coupled to a photometer. Different solutions were mixed by sequentially aspirating them via a selector valve into the syringe and subsequently circulating the resulting mixture to and from a mixing chamber. The $ABTS^{\cdot+}$-containing reagent solution was temporarily stored in one of the two mixing chambers. Absorbance values at 255 and 730 nm were quantified by dispensing the DOM sample or the reaction mixture from the syringe to a double-wavelength LED-photometer.

Yuan et al., 2019). For the EDC assay presented in this study (**Fig. 1a**), the $ABTS^{\cdot+}$-reagent solution was first prepared in bulk by adding 350 µL of chlorine solution (1 mM) per milliliter of ABTS solution (1 mM) which oxidized nominally 70% of the ABTS to $ABTS^{\cdot+}$ (i.e., $c_{ABTS^{\cdot+}}/(c_{ABTS^{\cdot+}} + c_{ABTS}) = 70\%$). Second, the UV absorbance of an undiluted DOM sample was measured at 254 nm as described above. Third, 2500 µL of a DOM sample (see Section 3.1.5 for the final DOC concentration) or DOM-free blank solution and 160 µL of pH buffer solution were added to a disposable cuvette with a 10-mm pathlength (4.5 mL, poly(methyl methacrylate), Brand, Germany). Subsequently, 540 µL of $ABTS^{\cdot+}$-reagent solution was added to the buffered sample solution. Fourth, the resulting absorbance at 728 nm was measured on a spectrophotometer after a reaction time of 15 min unless stated otherwise (see Section 3.1.2 for a discussion on the reaction time).

2.6.3. EDC analyzer

To automate liquid handling and absorbance measurements of the EDC assay, we developed a fluidic system coupled to a photometer (**Fig. 1b**). The fluidic system consisted of a syringe pump (Level-3 Cadent 3, IMI Precision, Switzerland) equipped with a single 2.5-mL zero-dead-volume syringe and a 12-way rotary selection valve (IMI Precision, Switzerland) as well as two mixing chambers which were connected to the selection valve. Both mixing chambers were built from vertically aligned 2.5-mL pipette tips (Amornthammarong et al., 2010). The detector was a double-wavelength LED photometer (Mikron 31, Runge, Germany) with a 10-mm pathlength and two LED-light source modules that emitted at wavelengths of 255 and 730 nm, respectively. The fixed wavelength of the LED modules led to a minor shift in the detection wavelength compared to the EDC assay and no correction was made for the molar absorption coefficient.

The EDC analyzer was programmed to replicate the four experimental steps of the EDC assay in a measurement cycle (**Fig. 1b**), during which one DOM-free blank and two DOM-containing samples were analyzed. This allows to determine the relative change in EDC and UV absorbance during ozonation (i.e., analysis of a DOM sample from (i) the ozonation-reactor influent and (ii) from the ozonation-reactor effluent). A measurement cycle consisted of the following steps: First, the $ABTS^{\bullet+}$-reagent solution was prepared by sequentially aspirating chlorine- and ABTS-containing solutions into the syringe. The resulting solution was then cycled five times from the syringe to the first mixing chamber and back. The mixing chamber was filled from the top and emptied from the bottom, resulting in an inversion of the syringe content, allowing for an efficient mixing (Amornthammarong et al., 2010). After a total of five mixing cycles, the entire $ABTS^{\cdot+}$-reagent solution was dispensed again to the mixing chamber for temporary storage. Second, the DOM-free blank solution was aspirated into the syringe and a fraction of this blank solution was dispensed to the photometer to zero the absorbance signals at both wavelengths. Third, buffer solution and an aliquot of the $ABTS^{\cdot+}$-reagent solution stored in the first mixing chamber were additionally aspirated into the syringe which still contained DOM-free blank solution. The syringe content was then cycled to and from the second mixing chamber. Fourth, the resulting mixture was passed through the photometer to measure the absorbance at 730 nm after a reaction time of 15 min. Subsequently, the steps two to four were repeated for the two DOM-containing samples to complete one measurement cycle. However, instead of zeroing the absorbance signal during the second step, the absorbance of the DOM samples was measured at 255 nm.

The EDC analyzer was controlled with a computer through an RS-232 communication line. Serial commands and system status were automatically sent and received, respectively, using a script written in Python (Version 3.7, Van Rossum and Drake, 1995). An additional Python script was used for data acquisition from the photometer. Both Python scripts are available at https://github.com/walpen/edc_analyzer.

2.6.4. Calculation of EDC from absorbance values

The EDC of a DOM sample (i.e., the number of electrons transferred from DOM to $ABTS^{\cdot+}$) was calculated based on the reductive loss of $ABTS^{\cdot+}$ in the reaction mixtures. We confirmed that $ABTS^{\cdot+}$ was primarily lost through reduction to ABTS by DOM in one-electron transfer reactions using SRFA as model DOM (see Section S1.6, SI). $ABTS^{\cdot+}$ concentrations were quantified based on measured absorbances at 728 or 730 nm using the molar absorption coefficient ε(728 nm, pH 7) = 14′000 $M^{-1}cm^{-1}$ (Walpen et al., 2016). To calculate the EDC, the residual $ABTS^{\cdot+}$ concentration in the reaction mixture containing DOM was compared to that of a reaction mixture containing only the DOM-free blank (i.e., ultrapure water) and normalized to the DOC concentration of the sample in the reaction mixture (Eq. (1))

$$\mathrm{EDC} = \frac{A_{blank} - A_{sample}}{l \cdot \varepsilon_{ABTS^{\cdot+}}} \cdot \frac{1}{c_{DOC}} \quad (1)$$

where A_{blank} and A_{sample} are the resulting absorbance values (λ = 728 or 730 nm) of the reaction mixtures containing the DOM-free blank and the DOM sample, respectively, $\varepsilon_{ABTS^{\cdot+}}$ ($M^{-1}cm^{-1}$) is the molar absorption coefficient of $ABTS^{\cdot+}$, l (cm) is the optical pathlength, and c_{DOC} ($mg_{DOC}\cdot L^{-1}$) is the DOC concentration in the final reaction mixture. For samples analyzed in replicates at increasing DOC concentrations, linear regression models were fitted to the measured residual $ABTS^{\cdot+}$ concentration versus the corresponding DOC concentration. The absolute value of slopes of the fitted models represented the EDC values (Eq. (2)).

$$c^{sample}_{ABTS^{\cdot+}} = -\mathrm{EDC} \cdot c_{DOC} + c^{blank}_{ABTS^{\cdot+}} \quad (2)$$

2.7. Quantification of micropollutants, bromide and bromate in wastewater samples

Residual concentrations of added micropollutants in secondary WWTP effluent samples were quantified on a high-performance liquid chromatograph (HPLC; LOQ: <0.02 µM, RSD: <1.2%, measurement range: 0.01–2 µM) coupled to a diode array and a fluorescence detector (UltiMate 3000, Thermo Scientific, Switzerland). Samples were separated on a C_{18} column (Cosmosil 5C_{18}-MS-II, 3 mm x 150 mm, 5 µm particle size, Nacalai Tesque, Japan) with a flow rate of 1 $mL\cdot min^{-1}$ using an isocratic eluent composed of 45% acetonitrile and 55% phosphoric acid (20 mM, pH 2).

Concentrations of bromide and bromate in secondary WWTP effluent samples were measured on an ion chromatograph (ICS-3000, Dionex, USA) equipped with an ion exchange column (AS9-HC, Dionex, USA) with an isocratic eluent containing sodium carbonate (9 mM) and sodium hydroxide (2 mM). Bromide concentrations were quantified after suppression by absorbance measurement at 200 nm (LOQ: 10 $\mu g\cdot L^{-1}$, RSD: 10%). Subsequently, bromate concentrations were quantified via a post-column reaction with iodide forming triiodide, which was detected by a second absorbance measurement at 352 nm (LOQ: 2 $\mu g_{\bullet}\cdot L^{-1}$, RSD: 10%; Salhi and von Gunten, 1999).

3. Results and discussion

3.1. Development and validation of the EDC assay

3.1.1. Effect of pH on the oxidation of ABTS by chlorine

The rate of oxidation of ABTS to $ABTS^{\cdot+}$ by chlorine decreases with increasing pH (Pinkernell et al., 2000). Because a fast, complete and reproducible preparation of $ABTS^{\cdot+}$ is critical for both methods presented herein, the EDC assay and the EDC analyzer, the kinetics and the stoichiometry of the formation of $ABTS^{\cdot+}$ was assessed photometrically in the pH range from 1 to 4. At a pH of 1.5 and 2.0, the reaction was completed within one minute (**Fig. S4**, SI) and the formed $ABTS^{\cdot+}$ subsequently remained stable for at least one hour (**Fig. S5**, SI). At pH values >2.0, the reaction was slower and incomplete (**Fig. S4**, SI). At pH 1.0, the reaction was fast but incomplete, presumably due a side reaction involving Cl_2 (Deborde and von Gunten, 2008). Therefore, $ABTS^{\cdot+}$-reagent solutions for all subsequent analyses were prepared by adding chlorine solution to an ABTS solution acidified with sulfuric acid resulting in a pH of 2.0 in the $ABTS^{\cdot+}$-reagent solution.

3.1.2. Reaction time of the EDC assay

To determine a suitable reaction time for the EDC assay, the evolution of the $ABTS^{\cdot+}$ concentration in EDC assay reaction mixtures with SRFA as a model DOM was assessed. For this purpose, the same volume of $ABTS^{\cdot+}$ reagent solution was added to a set of SRFA-containing solutions with increasing DOC concentrations and subsequently the resulting change in absorbance at 728 nm was measured over the course of 30 min. The absorption coefficient and hence the $ABTS^{\cdot+}$ concentration of the DOM-free reaction mixture (i.e., c_{DOC} = 0 $mg_{DOC}\cdot L^{-1}$) decreased slightly by 2.7% during the experiment (**Fig. 2a**), consistent with the previously observed instability of $ABTS^{\cdot+}$ at neutral pH conditions (e.g., Cano et al., 1998). Compared to this DOM-free reaction mixture, the decrease in $ABTS^{\cdot+}$ concentration of the reaction mixture containing SRFA was more pronounced and bi-phasic. The $ABTS^{\cdot+}$ concentration first decreased in an exponential and subsequently after approximately 15 min in a more linear fashion.

For every time point, the $ABTS^{\cdot+}$ concentration correlated linearly with the DOC concentration (shown for t = 15 min, inset of **Fig. 2b**). According to eq. (2), the absolute values of the slopes of these linear regression models represent the loss in $ABTS^{\cdot+}$ concentration per DOC concentration and therefore the EDC. The EDC increased rapidly up to approximately 15 min and subsequently continued to increase at a lower rate (**Fig. 2b**). However, no plateau was reached even for longer reaction times of up to 120 min (data not shown). This finding may be attributed to a presumably wide range of reactivities of electron-donating moieties in DOM towards $ABTS^{\cdot+}$. In addition, oxidation of phenolic moieties forms phenoxyl radicals. These radical species can form coupling products which may also donate electrons to $ABTS^{\cdot+}$ (Hotta et al., 2002, Hotta et al., 2001). As a consequence, a constant value may only be reached after much longer reaction times. Because of this lack of an obvious end point, an arbitrary time point of t = 15 min was selected for the quantification of EDC values for all subsequent analyses. This operationally defined reaction time of 15 min encompasses the rapid changes in $ABTS^{\cdot+}$ concentration during the first phase mentioned above. In addition, EDC values obtained for a set of model DOM isolate using the EDC assay with a 15-minute reaction time were in good quantitative agreement (see Section 3.1.6) to previously published EDC values quantified by MEO, where an electrochemical equilibrium was reached within approximately 60 min (Aeschbacher et al., 2012).

3.1.3. Interferences from selected dissolved inorganic species

Potential interferences of four inorganic species at concentrations relevant for wastewater on the resulting $ABTS^{\cdot+}$ concentration in the EDC assay were tested: manganese(II) (0–110 $\mu g\cdot L^{-1}$), iodide (0–125 $\mu g\cdot L^{-1}$), bromide (0–800 $\mu g\cdot L^{-1}$), and nitrite (0–4.6 $mg\cdot L^{-1}$; i.e., 0–1.4 $mg\text{-}N\cdot L^{-1}$). Among these inorganic species and in the absence of DOM, only iodide affected the $ABTS^{\cdot+}$ concentration (**Fig. S6**, SI). Iodide had an EDC value of 0.5 ± 0.2 $mol_{-}\cdot mol_{iodide}^{-1}$ after a reaction time of 15 min, suggesting a reduction of $ABTS^{\cdot+}$ by iodide. However, for DOM samples with DOC concentrations expected in the context of ozonation of secondary WWTP effluents (i.e., 3–10 $mg_{DOC}\cdot L^{-1}$), the contribution of iodide to the measured total EDC would be negligible compared to the contribution of DOM . For example, for an SRFA solution of 3 $mg_{DOC}\cdot L^{-1}$

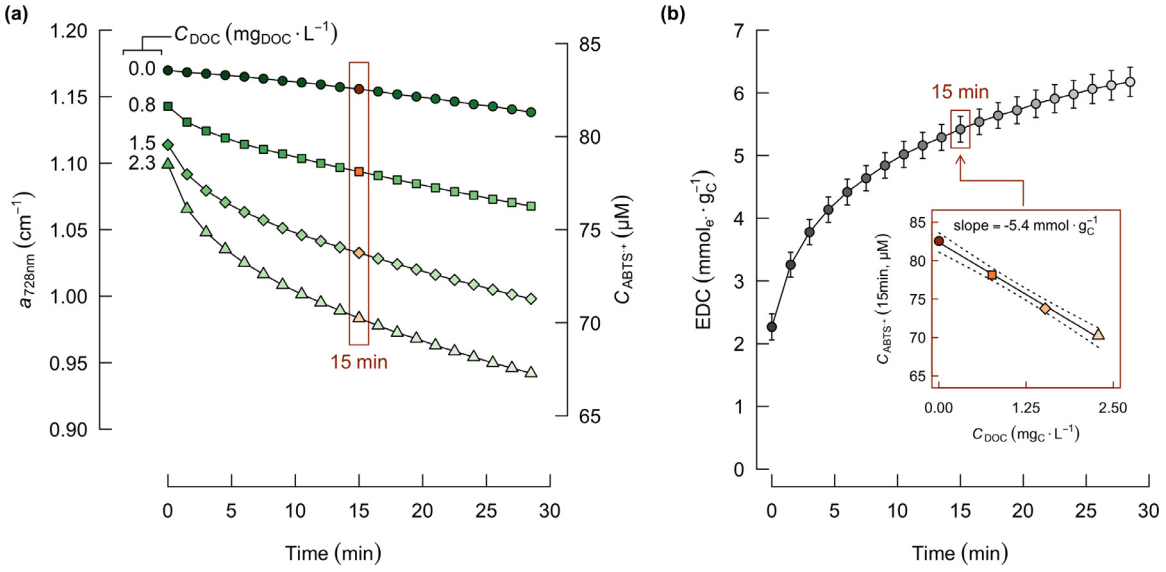

Fig. 2. (a) Decrease in the absorption coefficient a_{728nm} (cm^{-1}) of four EDC assay reaction mixtures containing increasing concentrations of Suwannee River fulvic acid (SRFA; c_{DOC} = 0.0–2.3 $mg_{DOC} \cdot L^{-1}$) over a reaction time of 30 min. The corresponding $ABTS^{\cdot+}$ concentrations (second *y*-axis) were calculated using the molar absorption coefficient of $ABTS^{\cdot+}$ of ε(728 nm) = 14′000 $M^{-1}cm^{-1}$ (Walpen et al., 2016). The red box indicates a reaction time of t = 15 min. (b) Increase in EDC of SRFA over time calculated from the linear regression models fitted to the $ABTS^{\cdot+}$ concentrations (panel a) versus the DOC concentration in the reaction mixtures. EDC values were determined as the absolute values of the slopes of these models. Inset: $ABTS^{\cdot+}$ concentration measured at a reaction time t = 15 min (red box in panel a) versus the DOC concentration of the reaction mixtures (according to eq. (2)). The slope of the linear regression model and the corresponding 95%-confidence intervals are indicated by the solid and dashed lines, respectively.

(EDC_{SRFA} = 5.14 $mmol_{e^-} \cdot g_C^{-1}$), a concentration of 125 $\mu g \cdot L^{-1}$ iodide would increase the EDC of this SRFA solution by only 4%. In contrast, manganese(II) and nitrite did not react with $ABTS^{\cdot+}$ in the absence of SRFA (**Fig. S6**, SI). However, in the presence of SRFA, increasing manganese(II) and nitrite concentrations resulted in increasing EDC values of SRFA (**Fig. S7**, SI). At the highest concentrations tested, i.e., at 110 $\mu g \cdot L^{-1}$ manganese(II) and 4.6 $mg \cdot L^{-1}$ nitrite, the measured EDC values of SRFA in the presence of these ions were elevated by 6% and 3%, respectively as compared to the EDC measured for SRFA without these ions. Iodide and bromide did not exhibit such effects. Taken together, these four investigated inorganic species will have a negligible effect on the EDC quantification if present below the tested concentrations.

We note that iron(II) associated with organic matter is oxidized in a one-electron transfer by $ABTS^{\cdot+}$ and therefore contributes to the measured EDC by 1 $mol_{e^-} \cdot mol_{iron(II)}$ (Lau et al., 2015). In cases where iron(II) is expected to be present in significant amounts (e.g., DOM sampled from anoxic environments), the contribution of iron(II) to the EDC may be accounted for by separately quantifying the iron(II) concentrations in sample aliquots. In secondary WWTP effluents, iron(II) is not expected to reach significant concentrations due to preceding oxic treatments.

3.1.4. Effects of the reduction potential E_H and initial $ABTS^{\cdot+}$ concentration on the measured EDC

The effects of the apparent reduction potential (E_H) and the initial $ABTS^{\cdot+}$ concentration on the measured EDC were systematically assessed in a series of EDC assays using SRFA as a model DOM. The E_H in the reaction mixtures is governed by the $ABTS^{\cdot+}$:ABTS concentration ratio according to the Nernst equation (e.g. Schwarzenbach et al., 2003, chap. 14). To assess the dependency of the measured EDC on the initial E_H, a series of EDC assays of SRFA with identical concentrations of $ABTS^{\cdot+}$, but increasing concentrations of ABTS were conducted. The calculated initial E_H values of these solutions ranged from +643 mV to +730 mV (see **Table S3**, SI). All reaction mixtures containing DOM-free blanks had similar residual $ABTS^{\cdot+}$ concentrations after a reaction time of 15 min (78.2 ± 1.2 μM, n = 8, mean ± standard deviation; **Fig. S8a**, SI). However, the EDC of SRFA determined in these reaction mixtures increased from 3.15 $mmol_{e^-} \cdot g_C^{-1}$ at an initial E_H of +643 mV to 5.48 $mmol_{e^-} \cdot g_C^{-1}$ at an initial E_H of +730 mV (**Fig. S8b**, SI). We attribute this effect to the broad distribution of apparent standard reduction potentials of phenolic or other electron-donating moieties present in DOM (Aeschbacher et al., 2012) and the resulting increasing thermodynamic feasibility or faster kinetics of the oxidation of these moieties by $ABTS^{\cdot+}$ with increasing E_H. These findings are consistent with a previous study in which the EDC of DOM quantified by mediated electrochemical oxidation increased with increasing E_H applied to the working electrode of the electrochemical analysis cell (Aeschbacher et al., 2012).

To test the effect of the initial $ABTS^{\cdot+}$ concentration, EDC assay reaction mixtures containing SRFA (c_{DOC} = 0–4 $mg_{DOC} \cdot L^{-1}$) and increasing initial $ABTS^{\cdot+}$ concentrations (35–140 μM) were prepared. The $ABTS^{\cdot+}$:ABTS concentration ratio was kept constant to maintain the same E_H in these reaction mixtures. The residual $ABTS^{\cdot+}$ concentration of the reaction mixtures containing DOM-free blanks ranged from 33 μM to 126 μM after a reaction time of 15 min (**Fig. S9a**, SI). The EDC of SRFA significantly increased with increasing initial $ABTS^{\cdot+}$ concentration from 4.1 ± 0.25 $mmol_{e^-} \cdot g_C^{-1}$ (initial $ABTS^{\cdot+}$ concentration 33 μM) to 5.41 ± 0.03 $mmol_{e^-} \cdot g_C^{-1}$ (initial $ABTS^{\cdot+}$ concentration 126 μM) (**Fig. S9b**, SI), highlighting the importance of an accurate preparation of the $ABTS^{\cdot+}$ reagent solution.

Overall, these findings suggest that the initial E_H and $ABTS^{\cdot+}$ concentration of the reagent solution have strong effects on the reaction kinetics or thermodynamics of the reduction of $ABTS^{\cdot+}$ by electron-donating moieties in DOM. To obtain reproducible EDC values, initial $ABTS^{\cdot+}$ concentrations have to be controlled accurately and changes in E_H over the course of the reaction should be minimized. Similar to a previous study (Walpen et al., 2016), we selected an initial E_H of +0.71 V for the EDC assay because this E_H is slightly above the standard reduction potential, E_H^0, of the redox couple $ABTS^{\cdot+}$:ABTS (i.e., E_H^0 = +0.68 V; Scott et al., 1993) thereby ensuring only small decreases in E_H over the course of the reaction (i.e., decreases in the $ABTS^{\cdot+}$:ABTS concentration ratio lead to

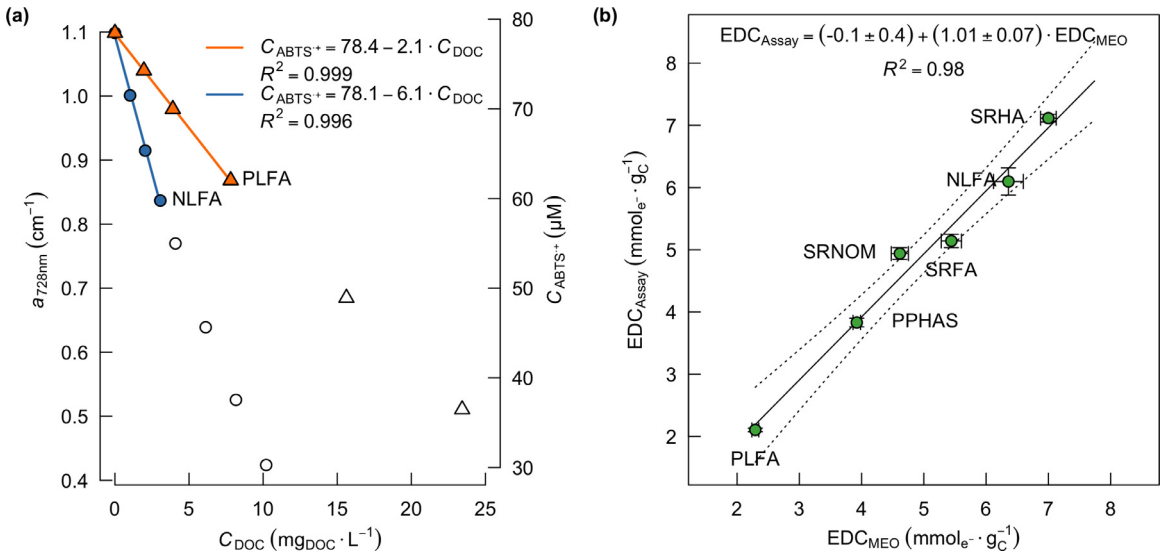

Fig. 3. Quantification of the electron donating capacity (EDC) of model DOM isolates. (a) Absorption coefficient a_{728nm} (cm^{-1}) of EDC assay reaction mixtures containing the model DOM isolate NLFA (filled and empty circles) or PLFA (filled and empty triangles) as a function of the respective dissolved organic carbon (DOC) concentrations of the two isolates (c_{DOC}). The absorbance values were measured after a reaction time of 15 min. The corresponding ABTS$^{\cdot+}$ concentrations ($c_{ABTS^{\cdot+}}$) are indicated by the second *y*-axis. The solid lines represent linear regression models fitted to the data that is plotted as filled symbols. The empty symbols indicate the data points that deviated from this linearity and were therefore excluded from the linear models. (b) EDC values of selected model DOM isolates quantified by the EDC assay compared to previously published EDC values of the same DOM isolates quantified by mediated electrochemical oxidation (MEO) (Aeschbacher et al., 2012). Error bars indicate standard deviations of at least triplicate measurements. The linear regression model and the corresponding 95%-confidence intervals are indicated by the solid line and dashed lines, respectively.

smallest E_H decreases around the $E_H{}^0$). A concentration of 87.5 µM was selected as initial ABTS$^{\cdot+}$ concentration, which yielded an absorption coefficient of 1.23 cm^{-1} at 728 nm.

3.1.5. Working range of the EDC assay

To assess the DOC concentration range that can be applied in the EDC assay, the upper limit of the working range and the limit of quantification (LOQ) were determined for two model DOM isolates, NLFA and PLFA. These isolates were selected because their EDC values were previously found to be high and low, respectively, compared to EDC values of other isolates. As expected, increasing DOC concentrations of both NLFA and PLFA resulted in decreasing absorption coefficients at 728 nm and thus decreasing ABTS$^{\cdot+}$ concentrations (**Fig. 3a**). The measured decreases followed linear trends at low DOC concentrations but deviated from linearity at higher DOC concentrations towards higher ABTS$^{\cdot+}$ concentrations. This deviation likely resulted from decreases in E_H over the course of the reactions, which become more pronounced as the reacting DOC concentrations increased (see discussion above). To determine the upper limit of the linear range for NLFA and PLFA, we fitted linear regression models to the corresponding ABTS$^{\cdot+}$ concentrations (**Fig. 3a**) and sequentially removed data points with the highest DOC concentration until the R^2-value of the model rose above a predefined threshold of 0.995. The upper limits of the linear ranges, i.e., the largest DOC concentrations of the models to first fulfill this condition (solid lines in **Fig. 3a**), were 3.1 and 7.8 mg$_{DOC}$·L^{-1} for NLFA or PLFA, respectively. The limit of quantification (LOQ = $a_{Blank} - 10 \cdot \sigma_{a,\,Blank}$ (Currie, 1999)) corresponded to a DOC concentration of 0.11 and 0.44 mg$_{DOC}$·L^{-1} for NLFA and PLFA, respectively. LOQ values are similar to those determined for the recently published methods for EDC quantification based on size-exclusion chromatography and flow-injection analysis (Önnby et al., 2018b; Walpen et al., 2016). Both of these methods were previously used to quantify the change in EDC of real wastewater samples upon chemical oxidation with chlorine and ozone. Taken together, we recommend diluting DOM-sample solutions to DOC concentrations between 0.5 and 3.0 mg$_{DOC}$·L^{-1} in the final reaction mixtures for routine analysis with the EDC assay.

3.1.6. Comparison of the EDC assay and MEO

To compare results obtained by the EDC assay to previously published values determined by MEO (Aeschbacher et al., 2012), six model DOM isolates were analyzed. For every isolate, a series of reaction mixtures containing increasing DOC concentrations ($n \geq 3$) was prepared and linear regression models were fitted to the residual ABTS$^{\cdot+}$ concentrations versus DOC concentration (**Fig. S10**, SI). Overall, the resulting EDC values (**Fig. 3b**) closely matched the EDC values obtained for the same isolates determined by MEO (slope = 1.01 ± 0.07, intercept = −0.1 ± 0.4, R^2 = 0.98).

3.2. Development and validation of the EDC analyzer

3.2.1. EDC quantification of a SRFA solution

An EDC analyzer was developed to automate liquid handling and absorbance measurements using a combined valve and syringe-pump system. Exemplary absorbance traces (λ_1 = 255 nm; λ_2 = 730 nm) over the course of one measurement cycle for the analysis of SRFA are shown in **Fig. S11** (SI). The UV absorption coefficient a_{255nm} of the tested SRFA solution was 0.181 ± 0.001 cm^{-1} (n = 2). Normalizing this value by the DOC concentration yielded a specific UV absorbance ($SUVA_{255}$) of 4.63 ± 0.02 L·(mg$_{DOC}$·m)$^{-1}$, which is in good agreement with a previously determined value of 4.4 L·(mg$_{DOC}$·m)$^{-1}$ (Walpen et al., 2016). As expected from the EDC assay, the addition of the ABTS$^{\cdot+}$ reagent to the SRFA solution resulted in a lower absorbance at 730 nm after a reaction time of 15 min compared to the DOM-free blank sample. This is caused by the electron transfer reactions from DOM to ABTS$^{\cdot+}$. The decrease in the absorption coefficient of 0.1686 ± 0.0005 cm^{-1} (n = 2) corresponded to a loss of 12.05 ± 0.04 µM ABTS$^{\cdot+}$. Normalizing this loss in ABTS$^{\cdot+}$ concentration by the DOC concentration yielded an EDC value of 4.8 ± 0.2 mmol$_{e-}$·g$_C^{-1}$ which is only slightly smaller than the value obtained from the EDC assay (i.e., 5.1 ± 0.1 mmol$_{e-}$·g$_C^{-1}$). A possible explanation for this small deviation as well as a systematic comparison of this value to previously published values to validate the EDC analyzer is provided in Section 3.2.2.

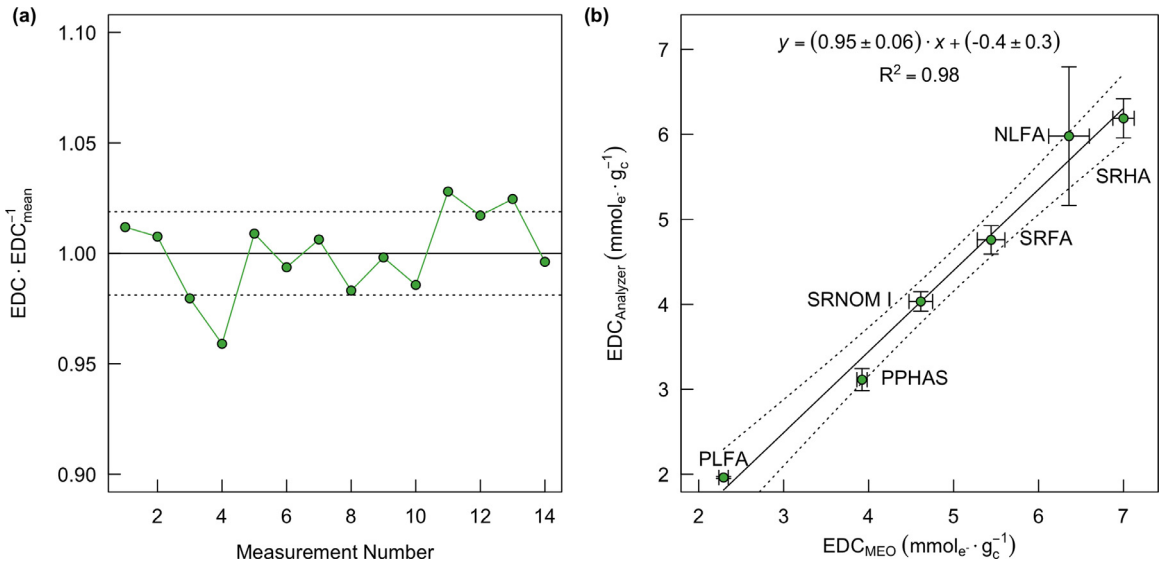

Fig. 4. (a) Electron donating capacity (EDC) values obtained for seven consecutive EDC measurement cycles of a single Suwannee River fulvic acid (SRFA) sample solution (c_{DOC} = 3.90 $mg_{DOC} \cdot L^{-1}$) relative to their mean value (n = 14). During each measurement cycle, the EDC of the same SRFA sample was measured twice. The relative mean value and the corresponding relative standard deviations are indicated by the solid and dashed lines, respectively. (b) EDC values of selected model DOM isolates quantified using the EDC analyzer compared to previously published EDC values of the same DOM samples quantified using mediated electrochemical oxidation (MEO) (Aeschbacher et al., 2012). Error bars indicate standard deviations of at least duplicate measurements. The slope of the linear regression model and the corresponding 95%-confidence intervals are indicated with the solid line and dashed lines, respectively.

The total duration of the measurement cycle was 74 min, during which the UV absorbance and the EDC values of two DOM samples were determined. We note that by optimizing the analysis sequence (e.g., by reducing the number of mixing cycles and rinsing steps, or by shortening of the reaction time), the analysis time for two samples may be shortened. However, since we considered the current analysis rate to be sufficient for detecting changes in sluggish systems such as WWTPs, we did not work towards shortening the duration of the measurement cycles.

3.2.2. Performance assessment of the EDC analyzer

The performance of the EDC analyzer was assessed by testing the repeatability of EDC and UV absorbance measurements of a single SRFA solution over a total of seven measurement cycles. The relative standard deviations of the EDC and UV absorption coefficients were both small with 1.9% (n = 14, **Fig. 4a**) and 0.003% (n = 14, **Fig. S12a**, SI), respectively.

Similar to the EDC assay, EDC values of six model DOM isolates were quantified using the EDC analyzer and compared to previously published EDC values of the same isolates obtained by MEO (Aeschbacher et al., 2012). The EDC values obtained using the EDC analyzer correlated linearly with the EDC values obtained by MEO (R^2 = 0.98, **Fig. 4b**) with a negative intercept of −0.4 ± 0.3 and a slope of 0.95 ± 0.06. These overall slightly lower EDC values obtained by the analyzer compared to those obtained by MEO and the EDC assay (see **Fig. 3b**) presumably reflect a slower mixing of the DOM sample and $ABTS^{\cdot+}$ reagent solution in the automated system resulting in a shorter reaction time in the EDC analyzer compared to the EDC assay. In the analyzer, solutions are sequentially aspirated into the syringe and subsequently delivered to a mixing chamber. Therefore, the solutions did not mix immediately due to differences in their densities. In contrast, solutions in the EDC assay are added to a cuvette and immediately mixed manually. The slight offset in the EDC values between the measurements may be eliminated by increasing the reaction time on the EDC analyzer. However, since the subsequent discussion is based on relative changes in EDC during ozonation, small offsets in absolute values are not expected to affect the data interpretation.

Table 1
Electron donating capacity (EDC) and absorption coefficient (a_{255nm}) of the three wastewater samples collected from (i) the ozonation-reactor influent, (ii) the ozonation-reactor effluent, and (iii) the post-ozonation sand-filter effluent of the Werdhölzli wastewater treatment plant in Zurich, Switzerland. The ozonation-reactor influent sample had a DOC concentration of 6.4 $mg_{DOC} \cdot L^{-1}$ and an estimated specific ozone dose of 0.6 ± 0.06 $mg_{O3} \cdot mg_{DOC}^{-1}$ was applied in the ozonation reactor at the time of sampling.

Sampling Point	EDC ($mmol_{e^-} \cdot g_C^{-1}$)	a_{255nm} (cm^{-1})
Ozonation-reactor influent	3.63 ± 0.08	0.115 ± 0.001
Ozonation-reactor effluent	1.39 ± 0.03	0.062±0.001
Sand-filter effluent	1.29 ± 0.03	0.060 ± 0.001

The accuracy of the UV measurements was tested by comparing the results obtained using the EDC analyzer to UV absorption coefficients obtained using a spectrophotometer (**Fig. S12b**, SI). The linear regression model fitted to the data had a slope of 1.05 ± 0.01 and an intercept which was not significantly different from zero. This small systematic bias was considered negligible and is not expected to affect relative changes in the UV absorbance.

3.3. Characterization of in- and effluent of an ozonation reactor by the EDC analyzer

To demonstrate the performance of the EDC analyzer with samples containing real DOM, filtered samples collected from the WWTP Werdhölzli in Zurich, Switzerland, were analyzed. The EDC of DOM from the ozonation-reactor influent was 3.68 ± 0.08 $mmol_{e^-} \cdot g_C^{-1}$ (see **Table 1**) and decreased by 62% to 1.39 ± 0.03 $mmol_{e^-} \cdot g_C^{-1}$ after passing the ozonation reactor with an estimated specific ozone dose of 0.6 ± 0.06 $mg_{O3} \cdot mg_{DOC}^{-1}$ (based on the measured DOC concentration and plant process data, **Fig. S3**, SI). This pronounced decrease in EDC reflects the oxidation of electron-donating moieties in DOM (primarily phenols) and is in good agreement with previous findings (Chon et al., 2015; Önnby et al., 2018b; Wenk et al., 2013). The sand filter only had a minor effect on the EDC which decreased by an additional 3% to 1.29 ± 0.03 $mmol_{e^-} \cdot g_C^{-1}$. The UV absorption coefficient a_{255nm} of

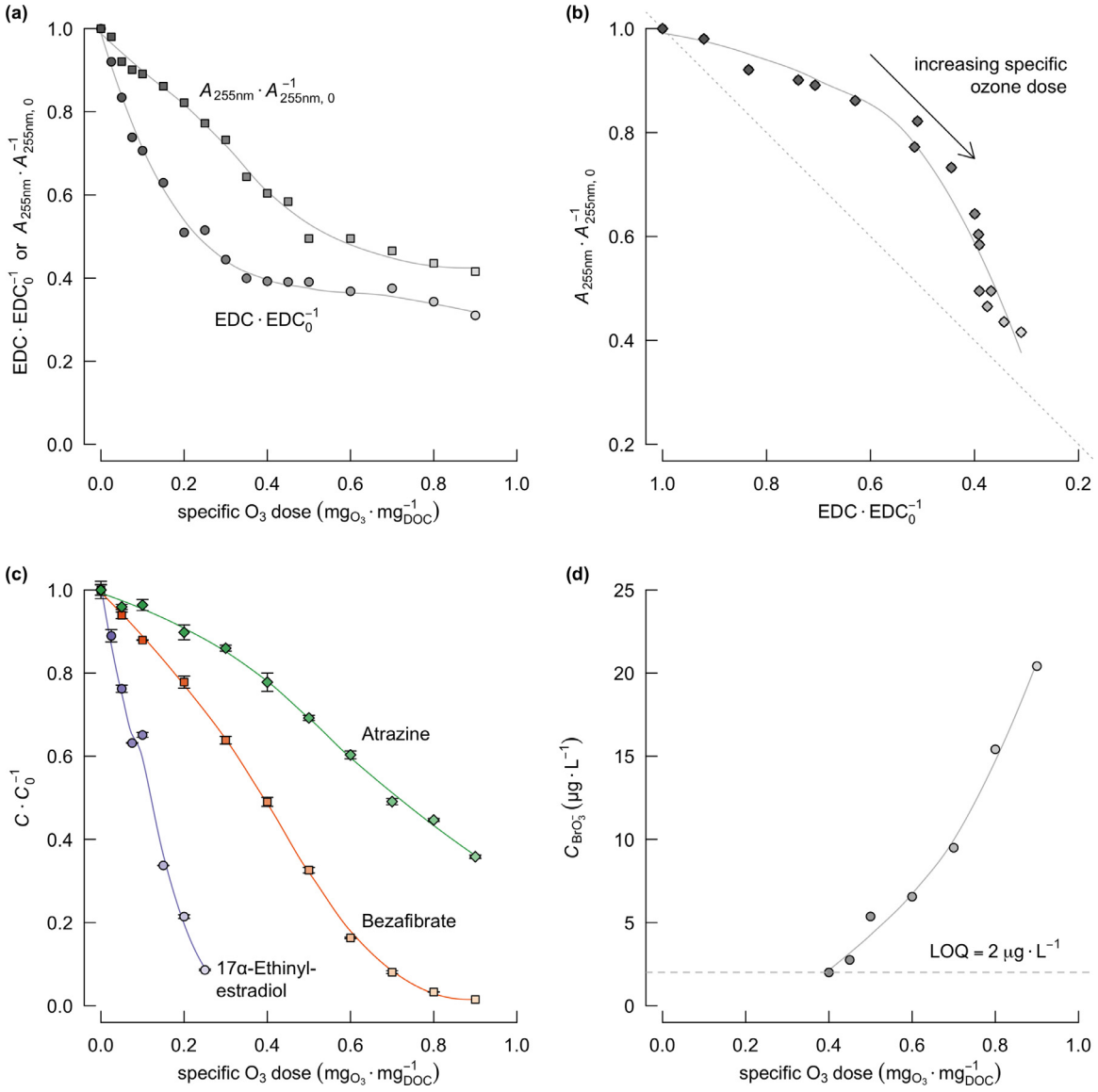

Fig. 5. Relative changes in the (a) electron donating capacity ($EDC \cdot EDC_0^{-1}$) and absorbance at 255 nm ($A_{255nm} \cdot A_{255nm,\ 0}^{-1}$) of a secondary WWTP effluent exposed to increasing specific ozone doses compared to the untreated sample. (b) The relative decrease in UV absorbance ($A_{255nm} \cdot A_{255nm,\ 0}^{-1}$, y-axis) from panel a replotted as a function of the relative decrease in EDC ($EDC \cdot EDC_0^{-1}$, x-axis). Residual concentrations (c) of 17α-ethinylestradiol (purple, filled circles), bezafibrate (orange, filled squares), and atrazine (green, filled diamonds) in the same wastewater relative to their concentrations in the untreated sample. (d) Increase in bromate concentration in the same samples. The wastewater sample was collected from the ozonation-reactor influent at the Werdhölzli wastewater treatment plant (Zurich, Switzerland) and had a pH of 7.9 before ozone addition. The addition of ozone stock solution diluted the DOC concentration and alkalinity to 5.5 $mg_{DOC} \cdot L^{-1}$ and 3.2 $mM_{HCO_3^-}$, respectively. The solid lines in panels (a–d) represent local polynomial regression models as a guide for the eye.

the ozonation-reactor influent sample was 0.115 ± 0.001 cm^{-1} and decreased by 44% to a value of 0.062 ± 0.001 cm^{-1} after passing the ozonation reactor and further decreased by 2% by passing the sand filter to 0.060 ± 0.001 cm^{-1} (**Table 1**; for full UV spectra see **Fig. S13**, SI). These findings clearly demonstrate that the high sensitivity of the EDC analyzer allows to detect the relative decrease in EDC and UV absorbance of real, secondary-treated wastewater DOM.

3.4. Laboratory ozonation of secondary WWTP effluent

3.4.1. Effect on EDC and UV absorbance

Increasing specific ozone doses (0–0.9 $mg_{O3} \cdot g_C^{-1}$) were added to DOM collected from the ozonation-reactor influent (Werdhölzli WWTP, Zurich, Switzerland) and the EDC analyzer was subsequently used to monitor the relative changes in EDC and UV absorbance compared to the untreated sample. Both parameters decreased with increasing specific ozone doses (**Figs. 5a**), consistent with the ozone-induced oxidation of electron-donating and chromophoric moieties in DOM (Wenk et al., 2013). The relative EDC showed a pronounced decrease at low specific ozone doses (<0.35 $mg_{O3} \cdot g_C^{-1}$, **Fig. 5a**). At a specific ozone dose of 0.35 $mg_{O3} \cdot g_C^{-1}$, the relative EDC decreased to 40%. Further increases in the specific ozone doses up to 0.9 $mg_{O3} \cdot g_C^{-1}$ resulted only in smaller additional decreases in the relative EDC down to 31%. The relative UV absorbance decreased to 60% and 42% at specific ozone doses of 0.35 and 0.9 $mg_{O3} \cdot g_C^{-1}$, respectively (**Fig. 5a**). Overall, the relative decrease in EDC was more pronounced compared to that in UV absorbance at low specific ozone doses (**Fig. 5b**). In contrast, the relative UV absorbance continued to decrease at higher doses and approximately matched the relative decrease in EDC at the highest applied specific ozone dose of

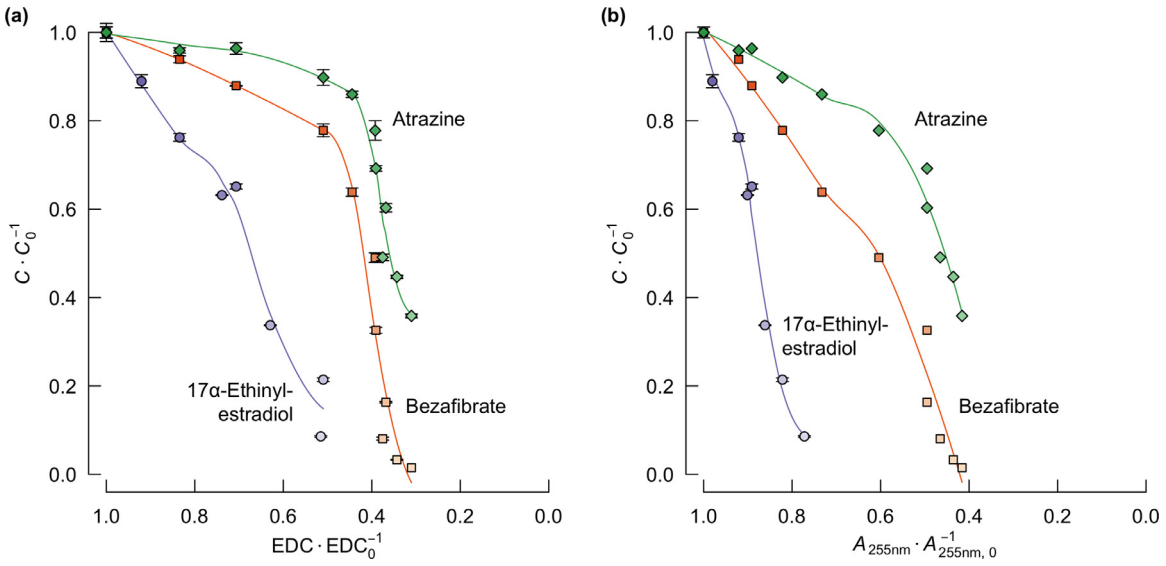

Fig. 6. Effects of ozone-induced oxidation on the relative concentrations of the three selected micropollutants (i.e., 17α-ethinylestradiol, bezafibrate, and atrazine) plotted versus the corresponding decreases in the relative residual (a) EDC ($EDC \cdot EDC_0^{-1}$) and (b) UV absorbance at 255 nm ($A_{255nm} \cdot A_{255nm,0}^{-1}$) of a secondary-treated wastewater sample. The data in both panels was re-plotted from Fig. 5. The solid lines in panels a and b represent local polynomial regression models as a guide for the eye.

0.9 $mg_{O3} \cdot g_C^{-1}$. This observation is consistent with previous findings and has been attributed to the oxidative transformation of phenolic moieties to chromophoric quinone moieties at low ozone doses and the subsequent oxidation of these quinones at higher ozone doses (Chon et al., 2015; Önnby et al., 2018a; Ramseier and von Gunten, 2009; Tentscher et al., 2018).

3.4.2. EDC and UV absorbance as surrogate parameters for micropollutant abatement and bromate formation

Fig. 5c shows the relative residual concentrations of the selected micropollutants (i.e., 17α-ethinylestradiol, bezafibrate, and atrazine) as function of specific ozone doses (0–0.9 $mg_{O3} \cdot g_C^{-1}$). As expected, the relative residual concentrations decreased with increasing specific ozone doses as a result of ozone-induced oxidation (Lee et al., 2014, 2013). Overall, micropollutant abatement was proportional to the apparent second-order rate constants (k_{O3}) of the reaction of these micropollutants with ozone at pH 7.9 (**Table S2**, SI). The relative residual concentration of 17α-ethinylestradiol ($k_{O3} = 1.2 \cdot 10^7\ M^{-1} \cdot s^{-1}$) decreased to 9% at a specific ozone dose of 0.25 $mg_{O3} \cdot g_C^{-1}$. In contrast, bezafibrate ($k_{O3} = 590\ M^{-1} \cdot s^{-1}$) required a higher specific ozone dose of 0.6 $mg_{O3} \cdot g_C^{-1}$ to reach a relative residual concentration of 16% and the concentration of atrazine ($k_{O3} = 6.0\ M^{-1} \cdot s^{-1}$) only decreased to 36% at the highest tested specific ozone dose of 0.9 $mg_{O3} \cdot g_C^{-1}$. Since ozone and secondarily formed hydroxyl radicals are the predominant oxidants (Buffle et al., 2006a) and because the second-order rate constants for the reactions of these micropollutants with hydroxyl radicals vary less than an order of magnitude ($9.8 \cdot 10^9$–$3.0 \cdot 10^9\ M^{-1} \cdot s^{-1}$, **Table S2**, SI), variations in abatement efficiencies are largely explained by the variations in k_{O3} of these micropollutants. Finally, bromate formation was observed at specific ozone doses >0.4 $mg_{O3} \cdot g_C^{-1}$ and increased abruptly from 2.0 to 20.4 $\mu g \cdot L^{-1}$ between 0.4 and 0.9 $mg_{O3} \cdot g_C^{-1}$ (**Fig. 5d**), consistent with the oxidation of bromide present in the untreated ozonation-reactor influent ($c_{Br^-} = 258 \pm 3\ \mu g \cdot L^{-1}$) by ozone and hydroxyl radical (von Gunten and Hoigné, 1994).

To assess the suitability of the relative decrease in EDC and UV absorbance as control parameters for ozonation, the relative micropollutant concentrations were replotted against the relative EDC (**Fig. 6a**) and relative UV absorbance (**Fig. 6b**). The relative concentration of 17α-ethinylestradiol decreased approximately linearly with decreasing relative EDC and reached a relative concentration of 9% while the relative EDC decreased to 52%. In contrast, concentrations of the less ozone-reactive micropollutants bezafibrate and atrazine showed smaller decreases to only about >78% for the same decrease in EDC. At higher specific ozone doses, bezafibrate and atrazine concentrations continued to decrease while additional decreases in EDC were small. In comparison, relative decreases in micropollutant concentrations were steeper and more linear when plotted against the relative decrease in UV absorbance similar to previous findings (Chon et al., 2015). Bromate concentrations sharply increased to >10 $\mu g \cdot L^{-1}$ for relative decreases in EDC and UV absorbance down to 34% and 44%, respectively (**Fig. S14**, SI). Overall, these results demonstrate that the EDC analyzer, which was designed for continual, long-term process monitoring, achieves a similar analytical performance and predictive power for micropollutant abatement as a previously presented laboratory method based on size-exclusion chromatography (Chon et al., 2015). Since the EDC of DOM was particularly sensitive to low ozone doses up to 0.4 $mg_{O3} \cdot g_C^{-1}$, monitoring changes in EDC absorbance may be specifically suited as control parameter for treatment processes requiring low ozone doses applied for example in combined ozonation and adsorption systems.

4. Conclusions

We developed and comprehensively validated (i) a photometric assay and (ii) an automated analyzer for the quantification of changes in EDC and UV absorbance of DOM during ozonation of secondary WWTP effluents. For this particular application, the two methods offer the following advantages over previous analytical systems:

- In the photometric EDC assay, the reagents, buffer and DOM sample solution are mixed directly in disposable cuvettes, which minimizes solution handling and residual $ABTS^{\cdot+}$-reagent concentrations are directly quantified using a photometer enabling fast and scalable EDC measurements.
- The design of the fluidic system of the EDC analyzer allows to perform continual, on-line EDC and UV analyses at a frequency of approximately two samples per hour. Compared to exist-

ing continuous-flow methods, this fluidic system uses lower reagent volumes and is fully automated. Furthermore, the use of only a single rotary valve and a single syringe pump in the EDC analyzer minimizes maintenance and costs.
- Analysis of model DOM isolates obtained with the EDC assay and the EDC analyzer are highly repeatable and closely match EDC values determined using established laboratory analysis methods such as MEO.
- The EDC analyzer will enable a continual monitoring of the relative decreases in EDC and UV absorbance during ozonation and potentially allow to predict micropollutant abatement.

Declaration of competing interest

The authors declare that they have no known competing financial interests or personal relationships that could have appeared to influence the work reported in this paper.

Acknowledgements

We thank U. Schönenberger (Eawag) for support with the quantification of micropollutants and C. Abegglen (Werdhölzli WWTP, ERZ Zurich) for providing wastewater samples and ozonation reactor process data. We further thank A. Joss and K. Villez (both Eawag) for helpful discussions. This project was financially supported by the Swiss Federal Office for the Environment (FOEN).

Supplementary materials

Supplementary material associated with this article can be found, in the online version, at doi:10.1016/j.watres.2020.116235.

References

Aeschbacher, M., Graf, C., Schwarzenbach, R.P., Sander, M., 2012. Antioxidant properties of humic substances. Environ. Sci. Technol. 46, 4916–4925.
Aeschbacher, M., Sander, M., Schwarzenbach, R.P., 2010. Novel electrochemical approach to assess the redox properties of humic substances. Environ. Sci. Technol. 44, 87–93.
Amornthammarong, N., Ortner, P.B., Zhang, J.-.Z., 2010. A simple, effective mixing chamber used in conjunction with a syringe pump for flow analysis. Talanta 81, 1472–1476.
Bader, H., Hoigné, J., 1981. Determination of ozone in water by the indigo method. Water Res. 15, 449–456.
Bahr, C., Schumacher, J., Ernst, M., Luck, F., Heinzmann, B., Jekel, M., 2007. SUVA as control parameter for the effective ozonation of organic pollutants in secondary effluent. Water Sci. Technol. 55, 267–274.
Bourgin, M., Beck, B., Boehler, M., Borowska, E., Fleiner, J., Salhi, E., Teichler, R., von Gunten, U., Siegrist, H., McArdell, C.S., 2018. Evaluation of a full-scale wastewater treatment plant upgraded with ozonation and biological post-treatments: abatement of micropollutants, formation of transformation products and oxidation by-products. Water Res. 129, 486–498.
Buffle, M.-.O., Schumacher, J., Meylan, S., Jekel, M., von Gunten, U., 2006a. Ozonation and advanced oxidation of wastewater: effect of O_3 dose, pH, DOM and $HO^{\cdot}$-scavengers on ozone decomposition and $HO^{\cdot}$ generation. Ozone Sci. Eng. 28, 247–259.
Buffle, M.-.O., Schumacher, J., Salhi, E., Jekel, M., von Gunten, U., 2006b. Measurement of the initial phase of ozone decomposition in water and wastewater by means of a continuous quench-flow system: application to disinfection and pharmaceutical oxidation. Water Res. 40, 1884–1894.
California Environmental Protection Agency, 2018. Policy for Water Quality Control for Recycled Water.
Cano, A., Hernández-Ruíz, J., García-Cánovas, F., Acosta, M., Arnao, M.B., 1998. An end-point method for estimation of the total antioxidant activity in plant material. Phytochem. Anal. 9, 196–202.
Chon, K., Salhi, E., von Gunten, U., 2015. Combination of UV absorbance and electron donating capacity to assess degradation of micropollutants and formation of bromate during ozonation of wastewater effluents. Water Res. 81, 388–397.
Chys, M., Audenaert, T.M., Deniere, W., Thérèse, E., Mortier, F.C., Van Langenhove, S., Nopens, H., Demeestere, I., W. H., K., Van Hulle, S., 2017. Surrogate-based correlation models in view of real-time control of ozonation of secondary treated municipal wastewater—model development and dynamic validation. Environ. Sci. Technol. 51, 14233–14243.
Currie, L.A., 1999. Nomenclature in evaluation of analytical methods including detection and quantification capabilities (IUPAC Recommendations 1995). Anal. Chim. Acta 391, 105–126.
Deborde, M., von Gunten, U., 2008. Reactions of chlorine with inorganic and organic compounds during water treatment—Kinetics and mechanisms: a critical review. Water Res. 42, 13–51.
Eggen, R.I.L., Hollender, J., Joss, A., Schärer, M., Stamm, C., 2014. Reducing the discharge of micropollutants in the aquatic environment: the benefits of upgrading wastewater treatment plants. Environ. Sci. Technol. 48, 7683–7689.
Federal Office for the Environment, 2018. Waters Protection Ordinance.
Gamage, S., Gerrity, D., Pisarenko, A.N., Wert, E.C., Snyder, S.A., 2013. Evaluation of process control alternatives for the inactivation of *Escherichia coli*, MS2 bacteriophage, and *Bacillus subtilis* spores during wastewater ozonation. Ozone Sci. Eng. 35, 501–513.
Gerrity, D., Gamage, S., Holady, J.C., Mawhinney, D.B., Quiñones, O., Trenholm, R.A., Snyder, S.A., 2011. Pilot-scale evaluation of ozone and biological activated carbon for trace organic contaminant mitigation and disinfection. Water Res. 45, 2155–2165.
Gerrity, D., Gamage, S., Jones, D., Korshin, G.V., Lee, Y., Pisarenko, A., Trenholm, R.A., von Gunten, U., Wert, E.C., Snyder, S.A., 2012. Development of surrogate correlation models to predict trace organic contaminant oxidation and microbial inactivation during ozonation. Water Res. 46, 6257–6272.
Hollender, J., Zimmermann, S.G., Koepke, S., Krauss, M., McArdell, C.S., Ort, C., Singer, H., von Gunten, U., Siegrist, H., 2009. Elimination of organic micropollutants in a municipal wastewater treatment plant upgraded with a full-scale post-ozonation followed by sand filtration. Environ. Sci. Technol. 43, 7862–7869.
Hotta, H., Nagano, S., Ueda, M., Tsujino, Y., Koyama, J., Osakai, T., 2002. Higher radical scavenging activities of polyphenolic antioxidants can be ascribed to chemical reactions following their oxidation. Biochim. Biophys. Acta - Gen. Subj. 1572 (1), 123–132.
Hotta, H., Sakamoto, H., Nagano, S., Osakai, T., Tsujino, Y., 2001. Unusually large numbers of electrons for the oxidation of polyphenolic antioxidants. Biochim. Biophys. Acta - Gen. Subj. 1526 (2), 159–167.
Huber, M.M., Göbel, A., Joss, A., Hermann, N., Löffler, D.S., McArdell, C., Ried, A., Siegrist, H., Ternes, T.A., von Gunten, U., 2005. Oxidation of pharmaceuticals during ozonation of municipal wastewater effluents: a pilot study. Environ. Sci. Technol. 39, 4290–4299.
Kaiser, H.-.P., Köster, O., Gresch, M., Périsset, P.M.J., Jäggi, P., Salhi, E., von Gunten, U., 2013. Process control for ozonation systems: a novel real-time approach. Ozone Sci. Eng. 35, 168–185.
Katsoyiannis, I.A., Canonica, S., von Gunten, U., 2011. Efficiency and energy requirements for the transformation of organic micropollutants by ozone, O_3/H_2O_2 and UV/H_2O_2. Water Res. 45, 3811–3822.
Knopp, G., Prasse, C., Ternes, T.A., Cornel, P., 2016. Elimination of micropollutants and transformation products from a wastewater treatment plant effluent through pilot scale ozonation followed by various activated carbon and biological filters. Water Res. 100, 580–592.
Lau, M.P., Sander, M., Gelbrecht, J., Hupfer, M., 2015. Solid phases as important electron acceptors in freshwater organic sediments. Biogeochemistry 123, 49–61.
Lee, Y., Gerrity, D., Lee, M., Encinas Bogeat, A., Salhi, E., Gamage, S., Trenholm, R.A., Wert, E.C., Snyder, S.A., von Gunten, U., 2013. Prediction of micropollutant elimination during ozonation of municipal wastewater effluents: use of kinetic and water specific information. Environ. Sci. Technol. 47, 5872–5881.
Lee, Y., Kovalova, L., McArdell, C.S., von Gunten, U., 2014. Prediction of micropollutant elimination during ozonation of a hospital wastewater effluent. Water Res. 64, 134–148.
Nanaboina, V., Korshin, G.V., 2010. Evolution of absorbance spectra of ozonated wastewater and its relationship with the degradation of trace-level organic species. Environ. Sci. Technol. 44, 6130–6137.
Önnby, L., Salhi, E., McKay, G., Rosario-Ortiz, F.L., von Gunten, U., 2018a. Ozone and chlorine reactions with dissolved organic matter - Assessment of oxidant-reactive moieties by optical measurements and the electron donating capacities. Water Res. 144, 64–75.
Önnby, L., Walpen, N., Salhi, E., Sander, M., von Gunten, U., 2018b. Two analytical approaches quantifying the electron donating capacities of dissolved organic matter to monitor its oxidation during chlorination and ozonation. Water Res. 144, 677–689.
Oulton, R.L., Kohn, T., Cwiertny, D.M., 2010. Pharmaceuticals and personal care products in effluent matrices: a survey of transformation and removal during wastewater treatment and implications for wastewater management. J. Environ. Monit. 12, 1956–1978.
Park, M., Anumol, T., Daniels, K.D., Wu, S., Ziska, A.D., Snyder, S.A., 2017. Predicting trace organic compound attenuation by ozone oxidation: development of indicator and surrogate models. Water Res. 119, 21–32.
Patel, M., Kumar, R., Kishor, K., Mlsna, T.U., Pittman, C., Mohan, D., 2019. Pharmaceuticals of emerging concern in aquatic systems: chemistry, occurrence, effects, and removal methods. Chem. Rev. 119, 3510–3673.
Pinkernell, U., Nowack, B., Gallard, H., von Gunten, U., 2000. Methods for the photometric determination of reactive bromine and chlorine species with ABTS. Water Res. 34, 4343–4350.
Pisarenko, A.N., Stanford, B.D., Yan, D., Gerrity, D., Snyder, S.A., 2012. Effects of ozone and ozone/peroxide on trace organic contaminants and NDMA in drinking water and water reuse applications. Water Res. 46, 316–326.
Prasse, C., Stalter, D., Schulte-Oehlmann, U., Oehlmann, J., Ternes, T.A., 2015. Spoilt for choice: a critical review on the chemical and biological assessment of current wastewater treatment technologies. Water Res. 87, 237–270.
Ramseier, M.K., von Gunten, U., 2009. Mechanisms of phenol ozonation—kinetics of formation of primary and secondary reaction products. Ozone Sci. Eng. 31, 201–215.

Salhi, E., von Gunten, U., 1999. Simultaneous determination of bromide, bromate and nitrite in low μg l^{-1} levels by ion chromatography without sample pretreatment. Water Res. 33, 3239–3244.
Schwarzenbach, R.P., Gschwend, P.M., Imboden, D.M., 2003. Environmental organic chemistry. Environmental Organic Chemistry, 2nd ed John Wiley & Sons, Inc., Hoboken, NJ, USA.
Scott, S.L., Chen, W.J., Bakac, A., Espenson, J.H., 1993. Spectroscopic parameters, electrode potentials, acid ionization constants, and electron exchange rates of the 2,2'-azinobis(3-ethylbenzothiazoline-6-sulfonate) radicals and ions. J. Phys. Chem. 97, 6710–6714.
Snyder, S.A., Wert, E.C., Rexing, D.J., Zegers, R.E., Drury, D.D., 2006. Ozone oxidation of endocrine disruptors and pharmaceuticals in surface water and wastewater. Ozone Sci. Eng. 28, 445–460.
Soltermann, F., Abegglen, C., Götz, C., von Gunten, U., 2016. Bromide sources and loads in Swiss surface waters and their relevance for bromate formation during wastewater ozonation. Environ. Sci. Technol. 50, 9825–9834.
Soltermann, F., Abegglen, C., Tschui, M., Stahel, S., von Gunten, U., 2017. Options and limitations for bromate control during ozonation of wastewater. Water Res. 116, 76–85.
Stapf, M., Miehe, U., Jekel, M., 2016. Application of online UV absorption measurements for ozone process control in secondary effluent with variable nitrite concentration. Water Res. 104, 111–118.
Tentscher, P.R., Bourgin, M., von Gunten, U., 2018. Ozonation of para-substituted phenolic compounds yields p-benzoquinones, other cyclic α,β-unsaturated ketones, and substituted catechols. Environ. Sci. Technol. 52, 4763–4773.
Ternes, T.A., Stüber, J., Herrmann, N., McDowell, D., Ried, A., Kampmann, M., Teiser, B., 2003. Ozonation: a tool for removal of pharmaceuticals, contrast media and musk fragrances from wastewater? Water Res. 37, 1976–1982.
Van Rossum, G., Drake, F.L.J., 1995. Python tutorial. Centrum voor Wiskunde en Informatica Amsterdam. Amsterdam, The Netherlands.
von Gunten, U., 2018. Oxidation processes in water treatment: are we on track? Environ. Sci. Technol. 52, 5062–5075.
von Gunten, U., Hoigné, J., 1994. Bromate formation during ozonization of bromide–containing waters: interaction of ozone and hydroxyl radical reactions. Environ. Sci. Technol. 28, 1234–1242.
von Sonntag, C., von Gunten, U., 2012. Chemistry of Ozone in Water and Wastewater Treatment: From Basic Principles to Applications. IWA Publishing, London.
VSA, 2020. List of planned and operational full-scale wastewater ozone reactors in Switzerland and Germany. Verband Schweizer Abwasser- und Gewässerschutzfachleute. https://www.micropoll.ch/anlagen-projekte/ozon/ (accessed 1.30.20).
Walpen, N., Schroth, M.H., Sander, M., 2016. Quantification of phenolic antioxidant moieties in dissolved organic matter by flow-injection analysis with electrochemical detection. Environ. Sci. Technol. 50, 6423–6432.
Wang, D., Bolton, J.R., Hofmann, R., 2012. Medium pressure UV combined with chlorine advanced oxidation for trichloroethylene destruction in a model water. Water Res. 46, 4677–4686.
Weishaar, J.L., Aiken, G.R., Bergamaschi, B.A., Fram, M.S., Fujii, R., Mopper, K., 2003. Evaluation of specific ultraviolet absorbance as an indicator of the chemical composition and reactivity of dissolved organic carbon. Environ. Sci. Technol. 37, 4702–4708.
Wenk, J., Aeschbacher, M., Salhi, E., Canonica, S., von Gunten, U., Sander, M., 2013. Chemical oxidation of dissolved organic matter by chlorine dioxide, chlorine, and ozone: effects on its optical and antioxidant properties. Environ. Sci. Technol. 47, 11147–11156.
Wert, E.C., Rosario-Ortiz, F.L., Snyder, S.A., 2009. Using ultraviolet absorbance and color to assess pharmaceutical oxidation during ozonation of wastewater. Environ. Sci. Technol. 43, 4858–4863.
Wittmer, A., Heisele, A., McArdell, C.S., Böhler, M., Longree, P., Siegrist, H., 2015. Decreased UV absorbance as an indicator of micropollutant removal efficiency in wastewater treated with ozone. Water Sci. Technol. 71, 980–985.
Wolf, C., Pavese, A., von Gunten, U., Kohn, T., 2019. Proxies to monitor the inactivation of viruses by ozone in surface water and wastewater effluent. Water Res. 166, 115088.
Yuan, Y., Zhang, H., Wei, Y., Si, Y., Li, G., Zhang, F., 2019. Onsite quantifying electron donating capacity of dissolved organic matter. Sci. Total Environ. 662, 57–64.
Zimmermann, S.G., Wittenwiler, M., Hollender, J., Krauss, M., Ort, C., Siegrist, H., von Gunten, U., 2011. Kinetic assessment and modeling of an ozonation step for full-scale municipal wastewater treatment: micropollutant oxidation, by-product formation and disinfection. Water Res. 45, 605–617.